Supplementary Information

Probing Coke Formation during Methanol-to-Hydrocarbon Reaction on Zeolite ZSM-5 Catalyst at the Nanoscale using Tip-enhanced Fluorescence Microscopy

Siiri Bienz,[1] Sophie H. van Vreeswijk,[2] Yashashwa Pandey,[1] Giovanni Luca Bartolomeo,[1] Bert M. Weckhuysen[2]* and Renato Zenobi,[1]* and Naresh Kumar[1]*

1 Department of Chemistry and Applied Biosciences, ETH Zurich, Vladimir-Prelog-Weg 3, 8093 Zurich, Switzerland

2 Inorganic Chemistry and Catalysis group, Department of Chemistry, Utrecht University, Universiteitsweg 99, 3584 CG, Utrecht, the Netherlands

Experimental details

Sample preparation: Large zeolite ZSM-5 crystals of size 100 x 20 x 20 μm^3 were obtained from ExxonMobil (Machelen, Belgium). Before performing the methanol-to-hydrocarbon (MTH) reaction, the zeolite crystals were calcined for 6 h at 550°C with a ramp of 5 °C/min. After calcination, drying was performed at 150°C for 30 min followed by a temperature increase to 550 °C under a 10 ml/min N_2 flow for 60 min. For each heating step, a ramp of 5 °C/min was used. Coking of the zeolite crystals was performed *via* the MTH reaction in a Linkam cell at 450 °C, with a 10 ml/min N_2 flow through a saturator with methanol. After performing the MTH reaction, the zeolite crystals were cooled down for 10 min. Pristine and coked ZSM-5 crystals placed on a Si substrate were characterized using Raman and fluorescence measurements at the micro and nanoscale.

Confocal Raman and fluorescence microscopy: The confocal Raman microscopy and fluorescence microscopy (CFM) were conducted on a top-illumination microscope (NT-MDT Spectrum Instruments, Russia). The instrument is equipped with a 632.8 nm He-Ne laser (LASOS, Germany) with a pinhole of 80 μm, a 100x, 0.7 NA objective lens (Olympus, Japan) and a EMCCD detector (Oxford Instruments, UK). Laser power was controlled using neutral density filters. The confocal hyperspectral CFM imaging was performed in an area of 30 × 30 μm^2 with a laser power of 20-55 μW on the sample and a spectrum integration time of 0.5 s. Whenever possible, measurements were performed on isolated zeolite crystals.

Preparation of Au coated probes: To prepare probes for tip-enhanced fluorescence (TEFL) imaging, Si atomic force microscopy (AFM) cantilevers (NanoAndMore, Germany) were first oxidized in a furnace (Carbolite Gero, UK) at 1000 °C for 23 h to increase the refractive index of the surface. Oxidized tips were cleaned in a UV-ozone cleaner (Ossila, UK) for 1 h. The cleaned tips were placed in a N_2 glovebox (MBraun, Germany) equipped with a built-in thermal evaporation system. Atomic force microscopy (AFM) cantilevers were coated with Au (99.99%, Acros Organics, USA) to a nominal thickness of 100 nm at a rate of 0.2-0.5 nm/s under 10^{-6} mbar pressure. To avoid any contamination, Au coated probes were stored in the N_2 glovebox having O_2 and H_2O concentration of < 0.1 ppm.

Tip-enhanced fluorescence microscopy: TEFL imaging was performed under ambient conditions using a top illumination system (NT-MDT Spectrum Instruments, Russia) equipped with an AFM, Raman spectrometer and CCD detector (Oxford Instruments, UK). A Ne-He laser (Spectra-Physics, Germany)) with a wavelength of 632.8 nm and a pinhole of 80 μm was focused on the sample using a 100x, 0.7

NA objective lens (Mitutoyo, Japan). TEFL spectra were measured Laser power using a laser power of 176 μW and an integration time of 0.5 s. The TEFL imaging was conducted in tapping mode AFM feedback in an area of 1 x 1 μm^2 in the central region of the crystal. AFM topography image was recorded simultaneously with the TEFL image.

Data analysis: In-house developed Python, R and R-studio codes were used for data analysis. AFM, fluorescence and TEFL imaging data was analysed using Gwyddion software. Polynomial line subtraction was applied to the Figures 3b, 3c, 4b and 4c. A zero-order background subtraction was performed on all spectra.

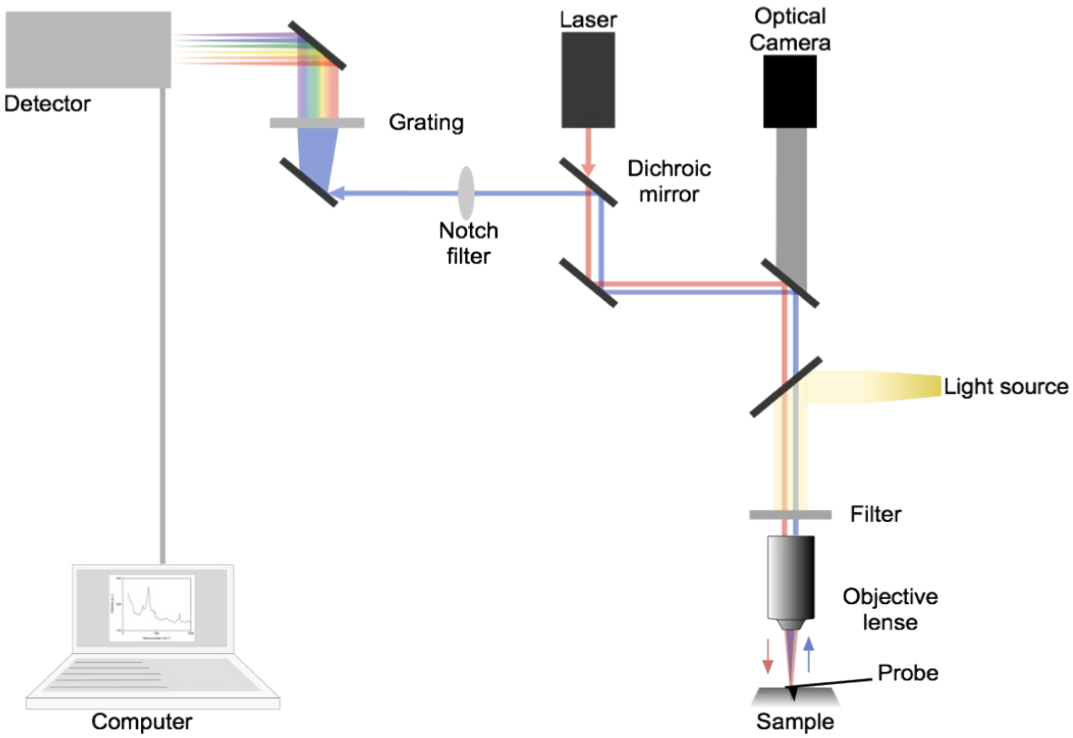

Figure S1. Schematic diagram of the optical setup used for the micro and nanoscale fluorescence measurements performed in this study.

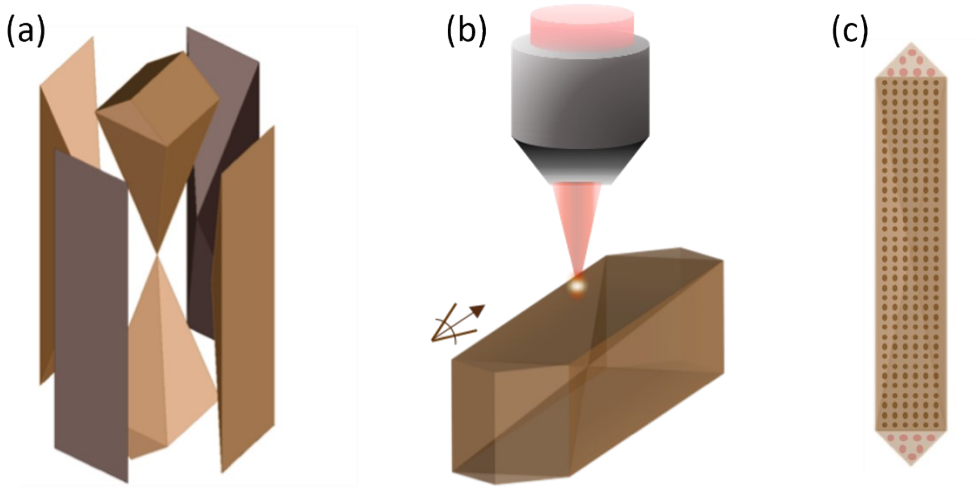

Figure S2. (a) Schematic illustration of the six pyramidal subunits that make up a zeolite ZSM-5 crystal. (b) Schematic diagram of the top illumination CFM imaging setup. The bright dot represents the focal spot of the 632.8 nm excitation laser. (c) Schematic depiction of the sinusoidal pores (brown) and straight pores (red) at the crystal surface.

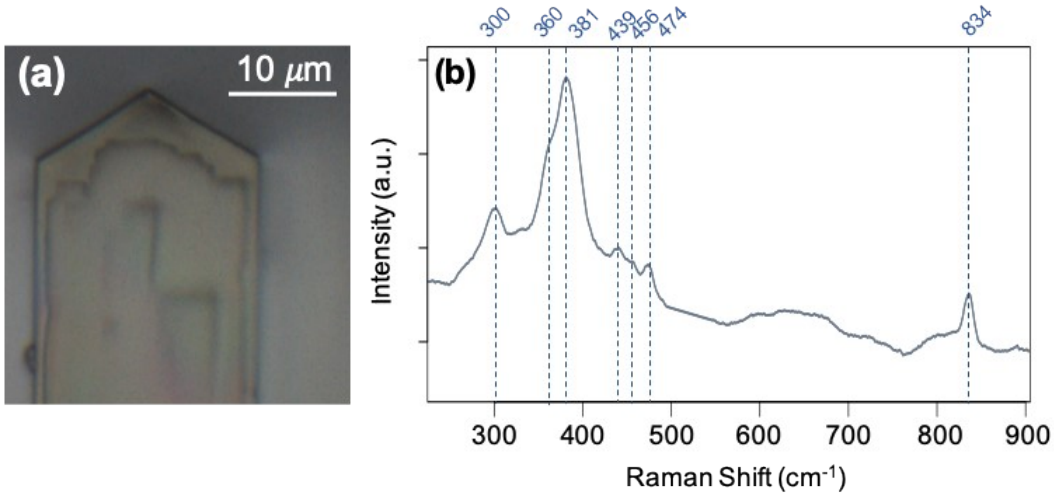

Figure S3. (a) Optical Image of a P-ZSM-5 crystal placed on a Si substrate. (b) Raman spectrum of the P-ZSM-5 crystal shown in (a) representing an average of 2500 spectra measured in a hyperspectral confocal Raman image. Prominent Raman vibrational modes of the zeolite crystal structure are highlighted.

Table S1. Assignment of the vibrational bands observed in the Raman spectrum of P-ZSM-5 crystal (Figure S3b). Notation: ν = stretching, δ = bending, s = symmetric, as = asymmetric, t = terminal, D6R = 6 membered double ring vibration.

Raman shift (cm^{-1})	**Band assignment**
300	δ(T-O-T)[1]
360	δ(D6R)[2]
381	ν_s(T-O-T)[3]
439	ν (Si-O-Si)[4]
456	δ(O-Si-O-(Al))[5]
474	δ(Si-O)[6]
834	Non-framework (Al-O)[7]

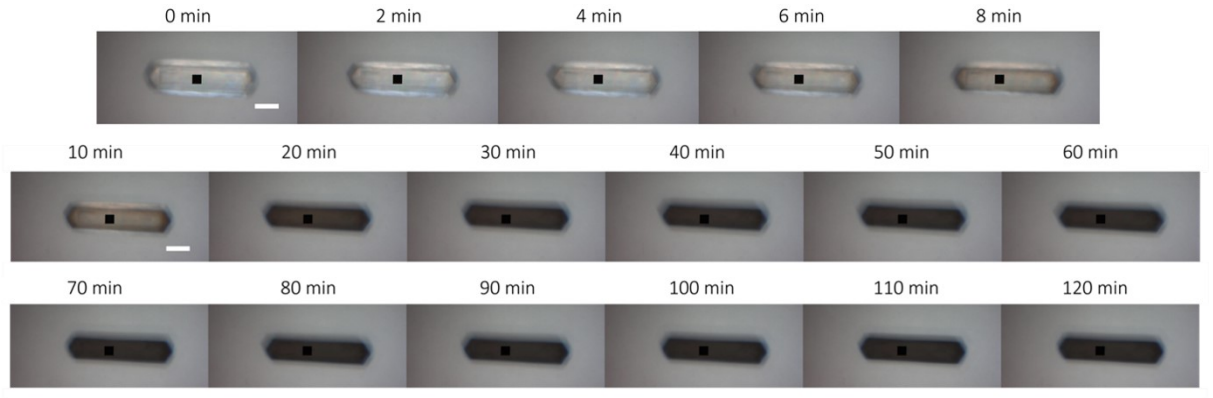

Figure S4. Optical microphotographs of a zeolite ZSM-5 crystal with increasing time-on-stream (TOS) until 120 min exposed to methanol during the MTH reaction. Scale bars: 20.8 μm. The crystal blackens progressively during the MTH reaction. The blackening starts quite gradually and becomes visual around 6 min. After 60 min, the zeolite crystal does not blacken any further indicating complete deactivation.

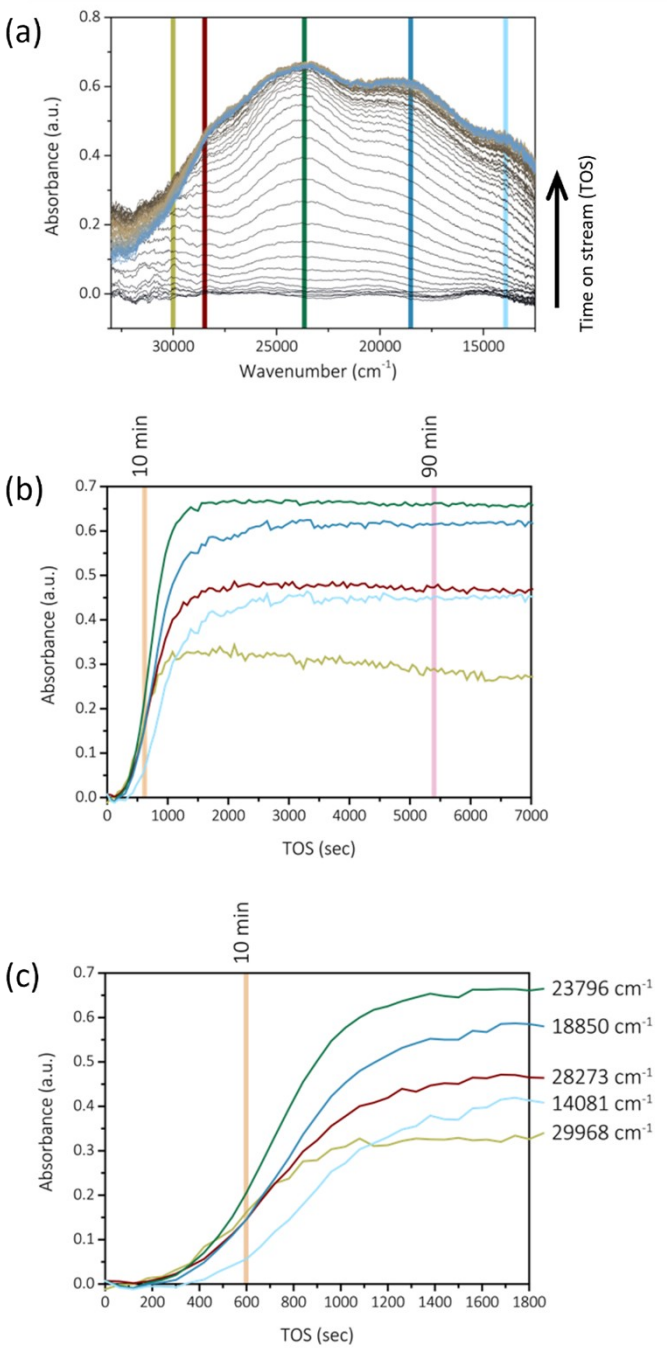

Figure S5. (a) Evolution of optical absorption spectra over time during the MTH reaction. Prominent absorption bands at ~ 14,100 cm^{-1} (due to charged and neutral poly-aromatics – more conjugated), 18,850 cm^{-1} (due to charged and neutral poly-aromatics), 23,800 cm^{-1} (due to charged alkylated naphthalene), 28,250 cm^{-1} (due to less alkylated benzenes) and 29,950 cm^{-1} (due to dienylic carbenium ions) are marked.[8, 9] A clear increase in the intensity of absorption bands between 35,000 and 10,000 cm^{-1} (or 286–1000 nm) is observed with increasing time-on-stream (TOS) is in-line with the catalyst darkening, as observed in the optical images in Figure S4. (b) Evolution of the marked absorption bands with increasing TOS until 116 min. (c) Evolution of the marked absorption bands with increasing TOS until 30 min.

At 10 min TOS, all absorption bands are still increasing, indicating that the aromatics are still changing/increasing. Particularly, the absorption assigned to the larger conjugated systems at ~ 14,100 cm^{-1} just starts to increase in intensity. After 60 min TOS, the absorption bands do not increase in their intensity any further, which is in agreement with the optical images. Consequently, 90 min TOS certainly represents a catalyst material containing a large amount of coke deposit and will certainly not show any further changes in its coke formation behaviour. Therefore, based on the UV-Vis spectroscopy measurements, the 10 min TOS sample represents a "working state" of the catalyst material, containing coke (precursor) species and the 90 min TOS

sample represents a “deactivated state” of the catalyst material, containing a large amount of graphite-like coke species on the zeolite surface.

Notably, the lifetime of the ZSM-5 catalysts used in this study is not directly comparable with the lifetime of commercially used ZSM-5 catalysts because of the following two reasons: Firstly, in this study we are using large ZSM-5 crystals as model catalyst. As many catalytic reactions largely depend on diffusion and the accessibility of the acidic and active sites in the zeolite structure, nano-sized zeolite crystals are often used as industrial catalyst due to higher activity and catalytic stability.[10-12] The downside, however, of these nano-sized zeolite crystals in fundamental zeolite research is that their visibility and thereby the possibility to obtain spatial information is limited due to the limitation of microscope resolution or, in the case of electron microscopy, beam damage.[13, 14] Therefore, large zeolite crystals have been of great interest as a model system to unravel the unique zeolite characteristics as well to prove the principle of novel methods of zeolite analysis.[14-18] However, this does mean that the larger size of the zeolite crystals leads to a faster deactivation and thereby shorter catalytic lifetime. Secondly, normally zeolites are tested in the MTH reaction in fixed or fluidised bed reactors in which at least 50 mg of catalyst is used. We coked our sample in a Linkam cell as we wanted to compare the coking behaviour over time on a single crystal level. The major changes in the set-up and the use of a significantly less amount of catalyst material further contribute to a faster catalyst deactivation.[19]

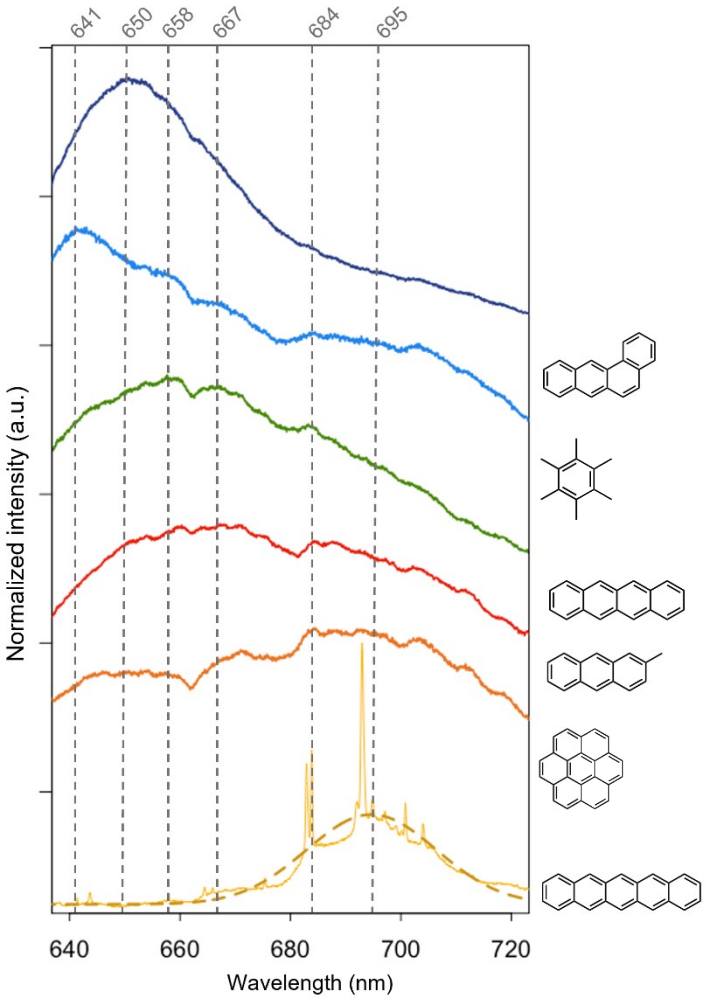

Figure S6. CFM spectra of some typical coke species proposed in the literature of the MTH process. The maxima of different fluorescence emission spectra are highlighted with a dashed line. Excitation laser: 632.8 nm. Integration time: 60 s. Spectra were normalized to the highest signal intensity and vertically shifted for easier visualization.

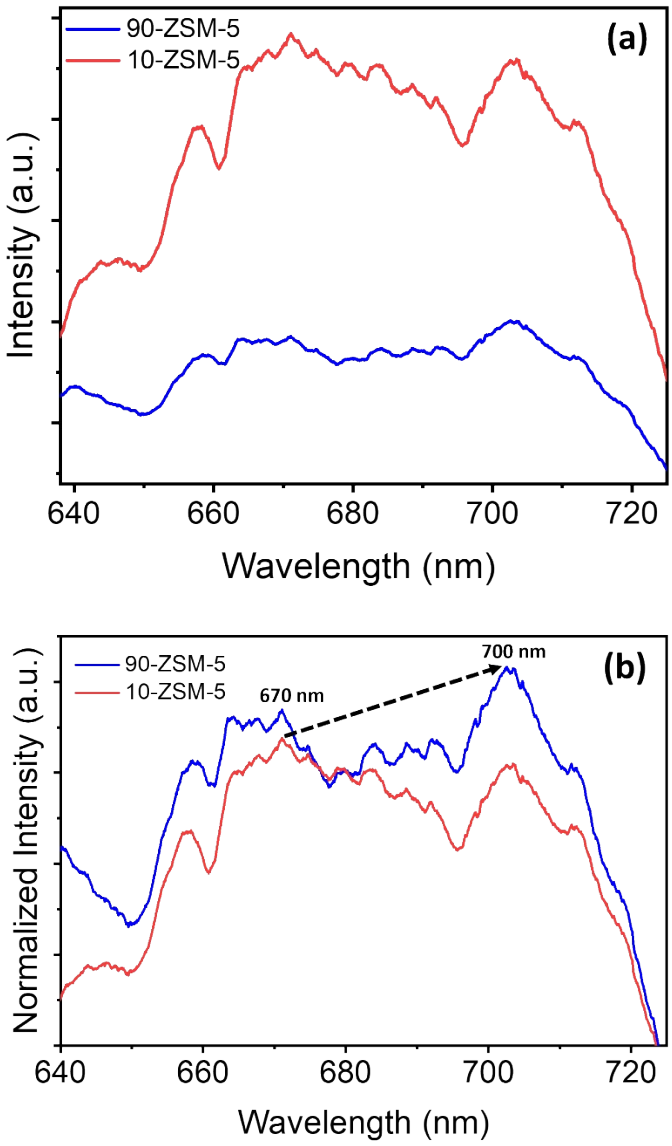

Figure S7. (a) Average spectra of the CFM images of the zeolite 10-ZSM-5 and 90-ZSM-5 catalysts shown in Figure 2. Each spectrum represents an average of 10000 CFM spectra. (b) Average CFM spectra of the zeolite 10-ZSM-5 and 90-ZSM-5 catalysts normalized to the signal in the middle of the spectrum at 680 nm.

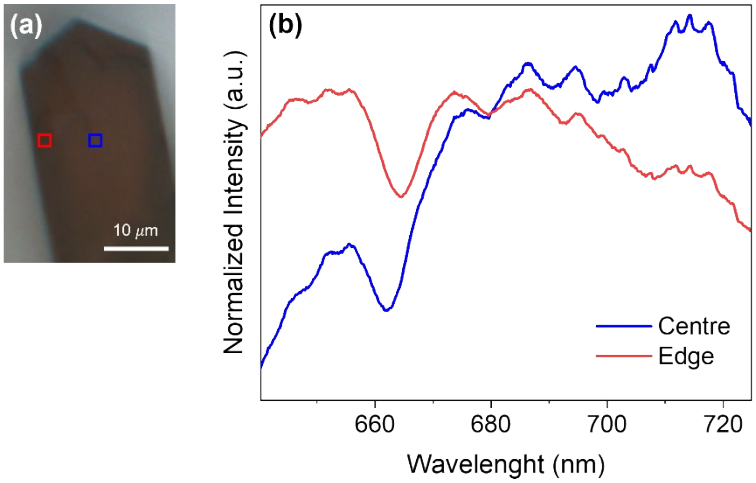

Figure S8. (a) Optical image of a 90-ZSM-5 crystal. (b) Average TEFL spectra measured in the centre and edge regions of the ZSM-5 crystal shown in (a). Each spectrum represents an average of 1600 individual TEFL spectra measured in an area of 1 μm^2. Both spectra have been normalised to the TEFL signal in the middle of the spectrum at 680 nm.

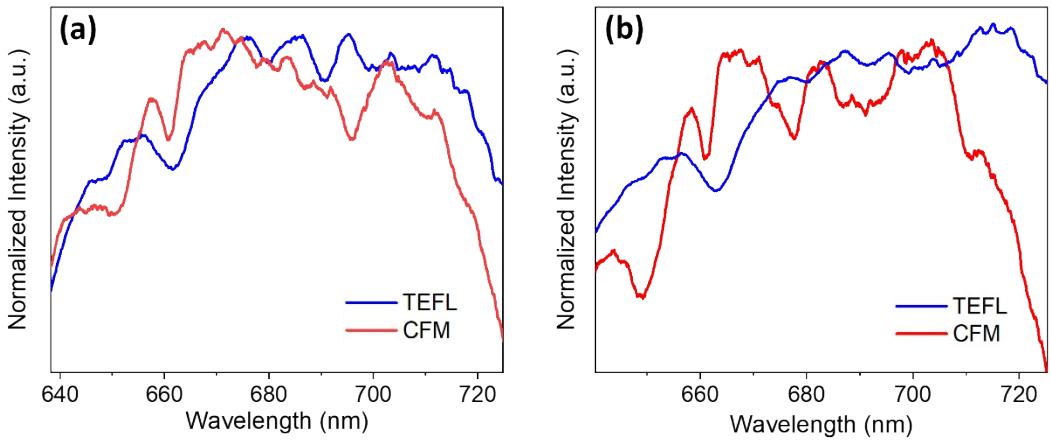

Figure S9. (a) Average fluorescence spectra measured in the TEFL image in Figure 3c and the centre of the CFM image (25 spectra, 1.5 μm^2 area) in Figure 2b of the 10-ZSM-5 crystals. (b) Averaged fluorescence spectra measured in the TEFL image in Figure 4c and the centre of the CFM image (25 spectra, 1.5 μm^2 area) in Figure 3b of the 90-ZSM-5 crystals. All spectra have been normalised to the signal in the middle of the spectrum at 680 nm.

Supplementary References

1. O. Attila, H. E. King, F. Meirer and B. M. Weckhuysen, *Chem. Eur. J.*, 2019, **25**, 7158-7167.
2. P. Knops-Gerrits, D. E. De Vos, E. J. P. J.P. Feijen and P. A. Jacobs, *Microporous Mater.*, 1997, **8**, 3-17.
3. P. K. Dutta and M. Puri, *J. Phys. Chem.*, 1987, **91**, 4329-4333.
4. R. Szostak, *Molecular Sieves: Principles of Synthesis and Identification*, Springer Science+Business Media, New York, 1989.
5. P. Bornhauser and G. Calzaferri, *J. Phys. Chem.*, 1996, **100**, 2035-2044.
6. S. R. Stojkovic and B. Adnadjevic, *Zeolites*, 1988, **8**, 532-535.
7. S. P. Zhdanov, T. I. Titova, L. S. Kosheleva and W. Lutz, *Pure Appl. Chem.*, 1989, **61**, 1977-1980.
8. J. Goetze, F. Meirer, I. Yarulina, J. Gascon, F. Kapteijn, J. Ruiz-Martinez and B. M. Weckhuysen, *ACS Catal.*, 2017, **7**, 4033-4046.
9. C. Vogt, B. M. Weckhuysen and J. Ruiz-Martinez, *ChemCatChem*, 2017, **9**, 183-194.
10. L. Yang, Z. Liu, Z. Liu, W. Peng, Y. Liu and C. Liu, *Chinese J. Catal.*, 2017, **38**, 683-690.
11. I. B. Minova, S. K. Matam, A. Greenaway, C. R. A. Catlow, M. D. Frogley, G. Cinque, P. A. Wright and R. F. Howe, *Phys. Chem. Chem. Phys.*, 2020, **22**, 18849-18859.
12. X. Niu, J. Gao, K. Wang, Q. Miao, M. Dong, G. Wang, W. Fan, Z. Qin and J. Wang, *Fuel Process. Technol.*, 2017, **157**, 99-107.
13. V. Ortalan, A. Uzun, B. C. Gates and N. D. Browning, *Nat. Nanotechnol.*, 2010, **5**, 506-510.
14. J. E. Schmidt, L. Peng, J. D. Poplawsky and B. M. Weckhuysen, *Angew. Chem. Int. Ed.*, 2018, **57**, 10422-10435.
15. J. E. Schmidt, L. Peng, A. L. Paioni, H. L. Ehren, W. Guo, B. Mazumder, D. A. Matthijs de Winter, O. Attila, D. Fu, A. D. Chowdhury, K. Houben, M. Baldus, J. D. Poplawsky and B. M. Weckhuysen, *J. Am. Chem. Soc.*, 2018, **140**, 9154-9158.
16. Z. Ristanovic, J. P. Hofmann, U. Deka, T. U. Schulli, M. Rohnke, A. M. Beale and B. M. Weckhuysen, *Angew. Chem. Int. Ed.*, 2013, **52**, 13382-13386.
17. X. Ye, J. E. Schmidt, R. P. Wang, I. K. van Ravenhorst, R. Oord, T. Chen, F. de Groot, F. Meirer and B. M. Weckhuysen, *Angew. Chem. Int. Ed.*, 2020, **59**, 15610-15617.
18. L. R. Aramburo, E. de Smit, B. Arstad, M. M. van Schooneveld, L. Sommer, A. Juhin, T. Yokosawa, H. W. Zandbergen, U. Olsbye, F. M. F. de Groot and B. M. Weckhuysen, *Angew. Chem.*, 2012, **124**, 3676-3679.
19. J. P. Hofmann, D. Mores, L. R. Aramburo, S. Teketel, M. Rohnke, J. Janek, U. Olsbye and B. M. Weckhuysen, *Chem. Eur. J.*, 2013, **19**, 8533-8542.